DETECTOR DEVELOPMENT FOR DYNAMIC PROTON RADIOGRAPHY

H.-J. Ziock, K. R. Alrick, R. A. Gallegos, J. Galyardt, N. T. Gray, G. E. Hogan, V. H. Holmes, S. A. Jaramillo, N. S. P. King, T. E. McDonald, Jr., K. B. Morley, C. L. Morris, D. M. Numkena, P. D. Pazuchanics, C. M. Riedel, J. S. Sarracino, G. J. Yates, J. D. Zumbro
[Los Alamos National Laboratory (LANL)]

M. Amman, JF. Beche, E. Beuville, V. Douence, L. Fabris, F. Goulding, N. Madden, J. Millaud, B. Turko, J. Walton, J. Zaninovich
[Lawrence Berkeley National Laboratory (LBNL)]

ABSTRACT

The development of high frame rate imaging charged particle detector systems for proton radiography at an advanced hydrotest facility (AHF) is discussed. The detector systems being developed are to be capable of providing a movie of dynamic events with inter-frame times as short as 200 nanoseconds and with spatial resolutions of 1/2 mm or better. Initial results from beam tests of a 1024 frame 8^2 pixel silicon detector prototype device and a four frame 1024^2 pixel electro-optically shuttered camera system will be presented.

INTRODUCTION

A promising new technology, proton radiography, for performing dynamic radiography on thick objects (100's of gm/cm^2) is being developed as part of the US Science Based Stockpile Stewardship program. The general concept of proton radiography (PRAD) is addressed in a separate paper in these proceedings[1]. In this paper we discuss the detector systems being developed for the PRAD project. The detector performance that we hope to achieve is given in Table 1. The detector development effort is broken into two separate parts. The first is aimed at providing limited multi-frame capability in a short time scale for rapid experimental verification of the PRAD concept. The second is longer term and addresses the full set of requirements given in Table 1, and if possible maintains a flexible design, capable of expanding to go beyond those requirements as they are likely to be a moving target. Before proceeding to the details of the detector development effort, we briefly review the basic detector options and their limitations.

Protons, being charged particles, themselves interact with the detector medium leaving an ionization trail that can be detected directly or indirectly. In ionization detectors, gaseous or solid state, the positively charged ions and negatively charged ions or electrons of the ionization track are separated and collected to form the signal directly. For silicon detectors it takes 3.6 eV of energy loss by the incident particle to generate one electron-hole (eh) charge pair on the average, although the fundamental energy loss mechanism for charged particles involve ~17 eV quanta[2]. The specific ionization energy loss for a minimum ionizing particle (MIP) in silicon results in an average of about 80 eh pairs per μm. The other means of signal generation is indirect, such as in a scintillator where the ionization is turned into light, which is collected and turned back into a second electric signal by, for instance, a photocathode or a photodiode. This entire process is rather inefficient, requiring on the order of 100 eV of energy loss in plastic scintillator to produce a photon which is difficult to collect and turn back into an electrical signal. The specific ionization in the plastic scintillator we used resulted in about 17,000 photons emitted into 4π steradians per cm of plastic scintillator for a MIP. Mirroring the back surface of the scintillator is at best only about 80% efficient so one can only achieve about 15,000 forward (into 2π steradians) photons.

Table 1: Detector Performance Goals	
Frames to be read out	~ 100 or more
Time spacing of frames	~ 200 nsec
Duration of frame (strobed)	~ 10 nsec
Spatial resolution at object	~ 1/4 mm pixel
Region to be imaged	~ 10 cm
Mass density accuracy	~ 1% or better
Particles detected / element	≥ 25,000
Maximum signal per pixel	~ 250k particles
Accuracy	~ 12 bit

LIGHT COLLECTION

Schematically a light based detector system for PRAD will resemble what is shown in Fig. 1. Light is generated in a scintillator, which is located in the image plane of the PRAD magnetic lens[3], reflected by

LA-UR-98-1015

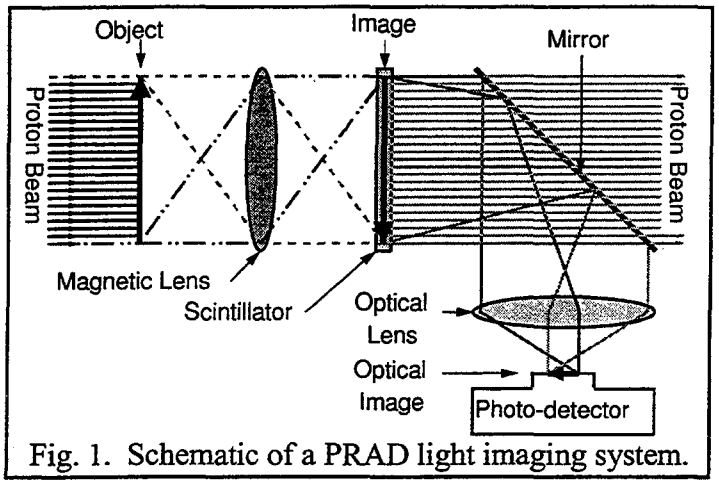

Fig. 1. Schematic of a PRAD light imaging system.

a 45° mirror out of the path of the proton beam, and then collected and imaged by an optical lens onto the photo-detector plane that creates the electrical signal. The above assumes that the photo-detector is itself sensitive to charged particles and must therefore be out of the proton beam. Although one could in principle use fiber optics to carry the light directly from the scintillator to the photo-detector, and thereby avoid the use of the mirror and lens, in practice this results in undesirable complications. First, the clear fiber array must have the same dimensions as the scintillator which according to Table 1 is on the order 10 cm on an edge if we assume that the magnetic lens is an identity lens. In bending the fibers at 90° to the beam direction, in order to get them out of the beam requires a depth for the clear fiber array of at least 1/2 the scintillator edge dimension and in reality it will be somewhat larger, especially if a 90° kink can't be made and instead one needs a smooth bend. These clear fibers will introduce a substantial amount of undesirable material in the beam creating background problems. This would severely limit the feasibility of using multiple planes of detector. The second problem is that Cerenkov light will be generated in the clear fibers. This becomes a problem as the fibers are being diverted to exit the region of the beam. At that point, light will be generated in clear fibers which are not connected to the ones that the proton will strike in the scintillating fiber array, resulting in an additional background problem. The Cerenkov problem can be minimized as the Cerenkov light is emitted in a forward direction and is broadband. This would however require the complication of using narrow bandpass filters for the scintillation light and choosing the proper fiber geometry.

Instead of trying to cope with all the problems associated with a fiber readout, we decided to use the mirror–lens coupled solution which has its own, but much more straight forward problem, namely the small amount of light captured by a lens system. This is especially true when the lens is operated with a magnification which is less than unity as is required when the photo-detector such as a microchannel plate (MCP), proximity focus diode (PFD), or CCD is much smaller in size than the object being imaged.

An optical lens system is used to form an image of the downstream face of the scintillating fiber array on the light detection device. The lens also serves the purpose of demagnifying the object to a size such that the image fits onto the detector. A lens does this rather inefficiently, capturing only a very small fraction of the light generated. The fraction of the light emitted in a forward direction (into 2π) that is captured by a lens which accepts a cone of half opening angle θ is simply

$$fraction = 1 - \cos(\theta). \quad (1)$$

Using various relationships for optics, the half cone acceptance angle for a lens system can be rewritten as

$$\theta = atan\{\, 1 / [2F(1 + 1/M)] \,\} \quad (2)$$

where F is the f - number (F#) of the lens (= focal length / effective diameter) and M is the magnification (typically less than unity in our application). Thus the fraction of forward light (0° to ±90°) accepted by a lens system from a point source is

$$fraction = 1 - \cos\{atan[M/(2F(1 + M))]\} \quad (3)$$

The angle θ is still not the half cone angle into which light is emitted by the scintillator, as the light is refracted to larger angles on leaving the high index scintillator into the air. The emission angle in the scintillator θ', which the lens accepts is thus considerably smaller than the already small acceptance half cone angle of the lens by an amount

$\theta' = asin\{[sin(\theta)]/n\}$, where n is the index of refraction of the fiber core (we take $n = 1$ for air). (4)

Putting this all together, one finds:

$$fraction = 1 - \cos\{asin[sin(atan\{ 1 /[2F(1 + 1/M)]\})/n]\} \approx (M^2) / [8n^2F^2 (1 + M)^2], \quad (5)$$

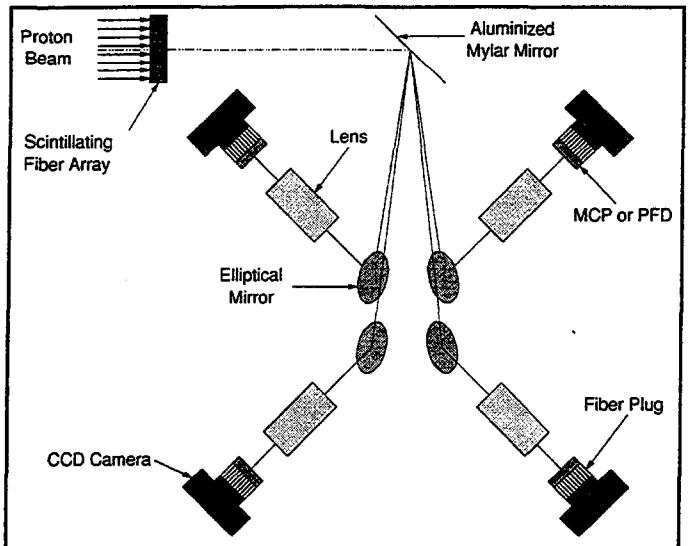

Fig. 2. Schematic of the 4-frame detector system. The cameras and lenses were in a common horizontal plane which was below the proton beam.

where the last result makes use of the small angle approximation for the trigonometric functions. Putting in values representative of those we used ($M = 1/5, F = 1.8, n = 1.6$) gives *fract* = 4 x 10^{-4}. This value is then further reduced by a number of other factors. These include a packing fraction associated with the active part of the scintillating fiber array (typically < 70%) and the light transmission of the optical system which is < 90%, especially for the blue light emitted by the scintillator. The largest factor is however the quantum efficiency of the light detector which is on the order of 20% for a photocathode and 35% for a CCD. When all the inefficiency factors are taken together, they reduce the overall efficiency of the system another factor of about 10. Taking the total number of forward photons, which in the case of a 2 cm scintillator for MIPs is 30,000 and multiplying by the lens acceptance and other inefficiencies results in about one detected photoelectron per proton and thus very poor counting statistics.

SHORT-TERM SOLUTION

In order to allow us to address a number of issues concerning multi-frame dynamic radiography we developed a limited frame camera system capable of recording images separated by 1 μs or less. Due to the limited development time available, we used off-the-shelf hardware. Our initial attempt involved the use of an IMCO ULTRANAC[4] framing camera. A framing camera consists of a photocatode from which the emitted electrons are accelerated and electrostatically focused to form an image on a downstream, long decay time phosphor screen. Horizontal and vertical electrostatic deflection plates between the photocathode and phosphor screen are used to move subsequent images to fresh locations on the phosphor screen. After some initial tests, this approach was discarded. We found the photocathodes in all our in-hand framing cameras (which were originally bought to be used in experiments dealing with the longer wavelength part of the visible spectrum) were nearly blind to the very blue light emitted by the standard plastic scintillators. Also the small diameter of the photocathode (18 mm diameter) required a reduced lens magnification resulting in even less light. We also had concerns about the potential for distortion in the image caused by space charge effects at the cross-over point of the electromagnetic lens in the framing camera. Stray magnetic fields from the proton imaging lens also distorted the framing camera image.

Our next attempt was based on a set of cooled slow scan CCD cameras, each coupled to a gated image intensifier for shuttering. The shuttering of the different cameras was time phased so that each camera recorded a different time (~ 40 ns burst of protons). The schematic of the camera system adopted is shown in Fig. 2. It should be noted that in this configuration each camera looks at an independent part of the solid angle, thereby avoiding any beam-splitter induced loss of light. The electronic shuttering is based upon our earlier work[5, 6] in electro-optic shuttering of microchannel plate image intensifiers (MCPIIs) by gating their photocathode emission. For some of the cameras we opted for proximity focus diodes[7] (PFDs), which we gated by switching their bias voltage on and off[8]. The intensifiers also provided gain for these weak photon flux experiments and provided wavelength shifting between input and output images for optimal spectral matching to the CCD. Because of the broad requirements for imaging camera system performance, such as wide dynamic range, variable gain, signal-to-noise, and tradeoffs between gain and resolution requirements, we decided to use both DEP[9] MCPII and Proxitronic PFD intensifiers, to exploit and evaluate the features of each type. The MCPIIs have higher gain and faster shuttering with lower high voltage and gate pulse amplitude requirements. The PFDs have higher QE, higher resolution and lower noise, but require much higher bias and gate potentials. Both have adequate dynamic range to

LA-UR-98-1015

effectively use the CCD pixel well capacity. We are still evaluating tradeoffs between the two intensifier types[10]. Results of a dynamic shot using this camera system are shown in Fig. 3, which shows the propagation of a detonation wave in a 28.5 mm radius piece of high explosive (HE).

LONG-TERM SOLUTION

For an AHF class detector system we took an approach which was modular in design and allowed for an evolving set of performance requirements. To demonstrate the basic concept we built a pair of 8 × 8 pixel detector systems designed to meet or exceed all the performance requirements given in Table 1, with the exception of pixel size. Our pixel sizes were $(1\ \text{mm})^2$ and $(0.5\ \text{mm})^2$. There is no problem with building

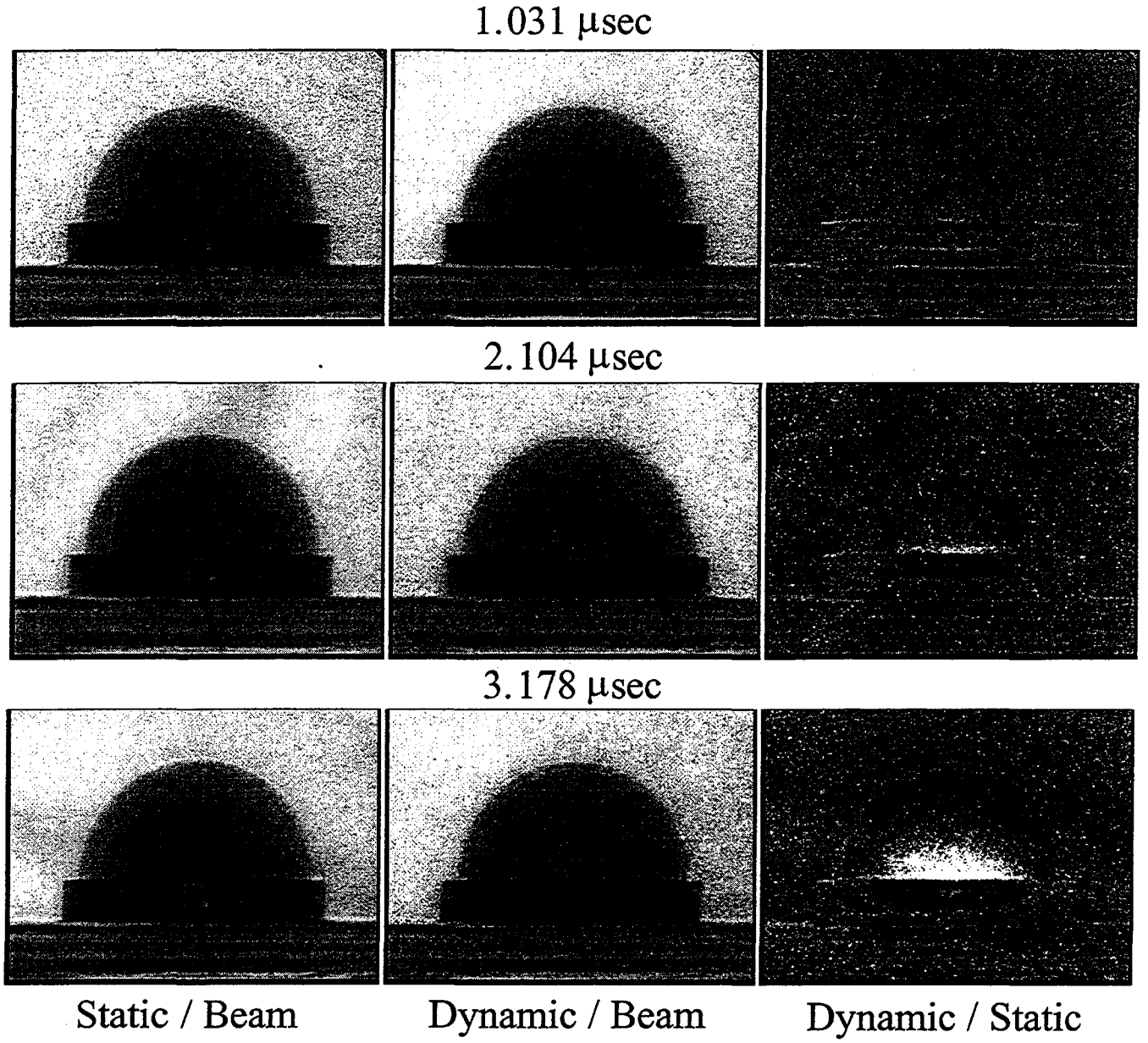

Fig. 3. Ratio images of proton radiographs taken by the detector system. Each row corresponds to a different camera. The fourth camera was unfortunately disabled by a lightning strike shortly before these radiographs were taken. The three different columns correspond to beam normalized radiographs of the static object (left column), beam normalized radiographs of the object as it was exploding (center column), and ratios of the dynamic to static images (right column), which emphasize differences between the static and dynamic radiographs. The given times are relative to detonator breakout.

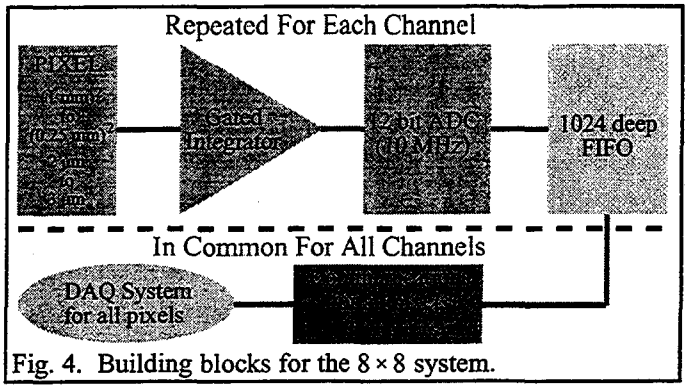

Fig. 4. Building blocks for the 8 × 8 system.

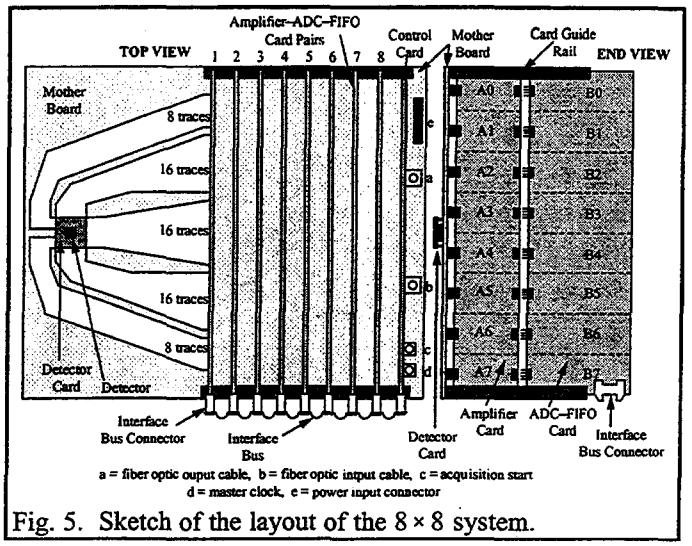

Fig. 5. Sketch of the layout of the 8 × 8 system.

smaller pixel sizes. The problem is instead in the high density interconnections which we were not prepared to address at this stage of the effort. The resulting small prototype was largely designed and constructed by LBNL.

The building blocks of the 8 × 8 system are shown in Fig. 4. For every pixel we had an individual low gain gated integrator, followed by a 10 MHz 12-bit pipelined ADC (Analog Devices AD9220), followed by a 1024 deep first in first out (FIFO) memory unit. In common to these 64 channels of electronics was a control card. This provided the proper phasing of the clock signal which was derived from the accelerator RF system, the trigger signal that started the data storage in the FIFO's and the readout circuitry that read back the 1024 readings from each of the 64 FIFO's. Each reading was then sent via a fiber optic link to the data acquisition computer on command via a CAMAC card once the exposure set was complete. The entire system was built using discrete off-the-shelf components. The hardware configuration is shown in more detail in Fig. 5 and was centered around a Motherboard into which we could plug different samples of the 8 × 8 detector. Into the Motherboard we also plugged 8 pairs of cards, each card pair servicing 8 pixels. The card pairs consisted of the gated integrator / driver card which in turn fed the ADC-FIFO card. The 9th card that plugged into the Motherboard was the control card mention above. A schematic of the gated integrator is shown in Fig. 6.

The silicon *pin* detectors themselves were of a very special design which made use of epitaxial processing by Lawrence Semiconductors[11]. The detectors were made effectively very thin because we were concerned about the potential for collapse of the detector bias field and the very large current spikes that might have otherwise occurred when on the order of 100,000 protons hit each and every pixel every proton burst. The detectors consisted of a 500 μm thick very heavily *n*-doped silicon substrate (few × 10^{19} dopant atoms/cc), on top of which a 2 or 3 μm thick epitaxial layer of more lightly doped *n*-type material (~10^{15} dopant atoms/cc) was grown, and which during operation formed the active (*i*-type) part of the detector. Doping profiles of two of the wafers are shown in Fig. 7. Ion implanted *p*-type regions were

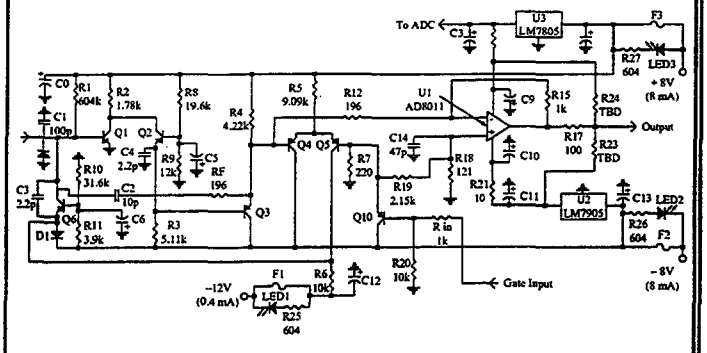

Fig. 6. Schematic of the gated integrator. The charge gain for the amplifier is about a factor of 5.

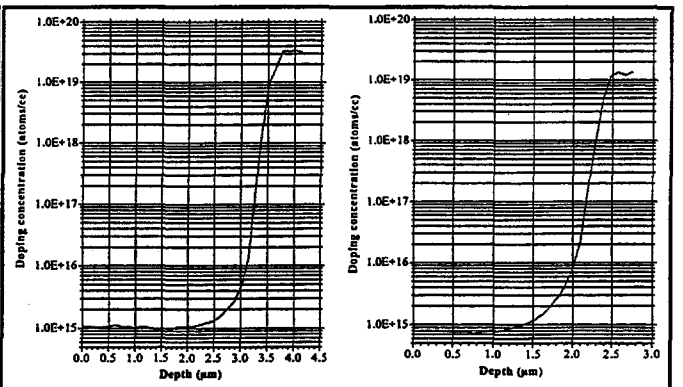

Fig. 7. Doping profiles for one of the 3 μm and one of the 2 μm epitaxial detector wafers.

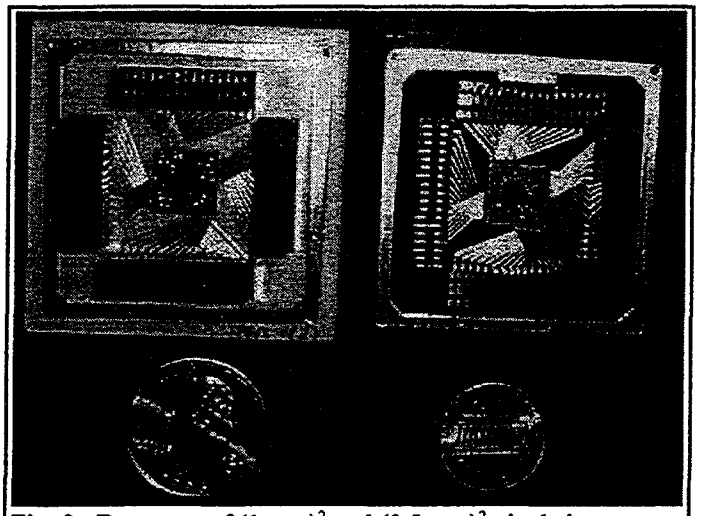

Fig. 8. Detectors of (1 mm)^2 and (0.5 mm)^2 pixel sizes.

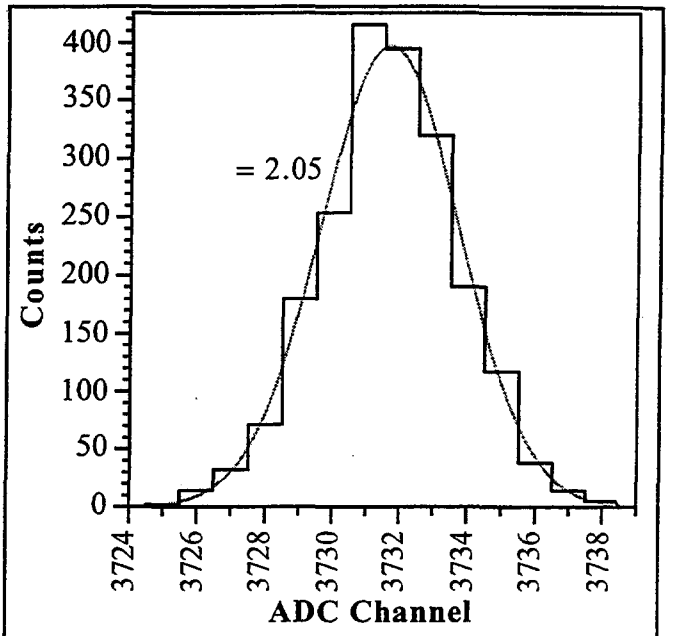

Fig. 9. System performance at 5 MHz with DC input.

then used to make the individual pixels. These were in turn sputtered with aluminum contacts to which the wire bonds were made. The detectors were glued to small ceramic cards (Fig. 8) which had connectors along their periphery to allow them to be plugged into the Motherboard. Despite the thinness of the active detector layer, substantial signals (160 to 240 eh pair on average) were generated for each proton, which is to be compared to the single photoelectron per proton from the scintillator based system discussed earlier. The detectors were biased at a few volts, with the bias being applied to the substrate side. The pixels side was connected to the electronics, which was designed to offer a very low input impedance up to very high frequencies. (Subsequent measurements showed that the epitaxial (active) layer of the detectors was fully depleted by the internal junction voltage.)

Leakage currents across the detector wafers varied. Occasional pixels showed leakage currents in the 10 μA range. However, sub-nanoamp values were far more common and a number of 8 × 8 pixel regions were found on the wafers in which all the pixels had sub-nanoamp leakage current values. For comparison, the proton beam induced signal currents in the pixels were in the 10 to 100 μA range.

The performance of the detectors and readout electronics is shown in Figs. 9 to 14. Fig. 9 shows the performance during a bench test of the electronics chain when it was clocked at 5 MHz with a DC voltage level through a resistor providing the injected input charge. The rms deviation is ~2 ADC counts, (4095 = full scale). A similar noise level was seen with the system in the experimental area and reading out a detector just before or after beam bursts arrived. Fig. 10 shows the linearity of the system response averaged over all 64 pixels as a function of proton beam intensity. The horizontal axis gives the proton beam intensity as measured by a toroidal pickup coil (arbitrary scale units with an obvious zero offset) and the vertical axis gives the 64 pixel average ADC value. The spread in the points is largely due to noise in the pickup coil circuit. Fig. 11 shows the time response of the system. The 800 MeV proton beam at the Los Alamos Neutron Scattering Center (LANSCE) for our tests was run in a chopped mode with a frequency of 1/72 of the fundamental accelerator frequency of 201.25 MHz resulting in a chopped beam burst once every ~ 358 ns. The 358 ns mode could be further gated to give a proton burst once every N x 358 ns (N = integer). For Fig. 11, two detector response curves are shown, one with N=2 and the other with N=10. The detector system itself took readings once every 358 nsec. As can be seen, the detector responded fully to the beam time structure. Fig. 12 shows a picture of a vertical resolution pattern taken with a (0.5 mm)^2 pixel detector. The object imaged consisted of 1/2 mm wide slots with a pitch of 1 mm cut into a heavy metal plate. The resolution pattern was placed in the object plane of the magnetic lens system of our radiography setup[1]. The detector plane coincided with the image plane of the magnetic lens and immediately downstream of it we placed a phosphor image plate. The relative alignment of the detector and resolution pattern can be seen in the image plate picture (the left half of Fig. 12). The central

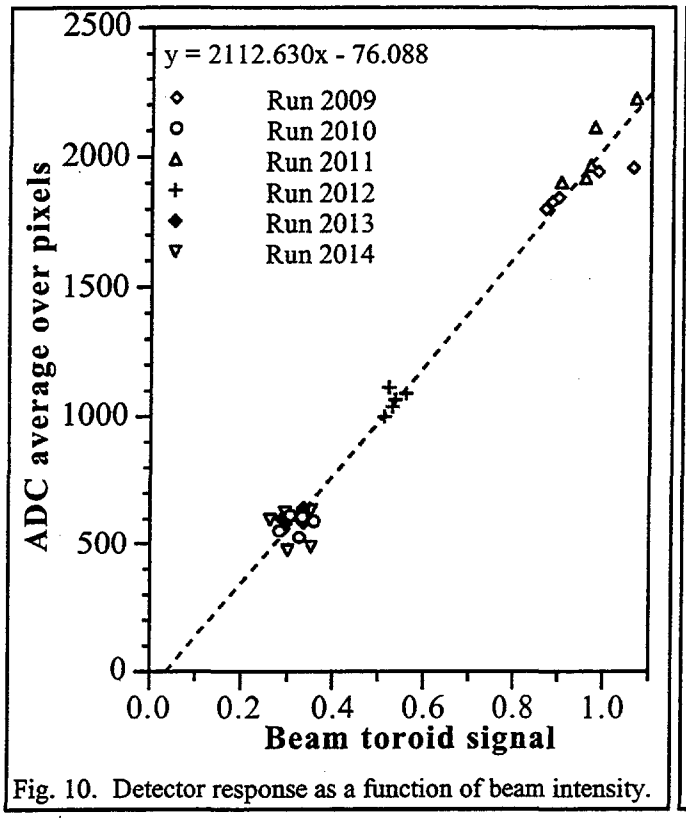

Fig. 10. Detector response as a function of beam intensity.

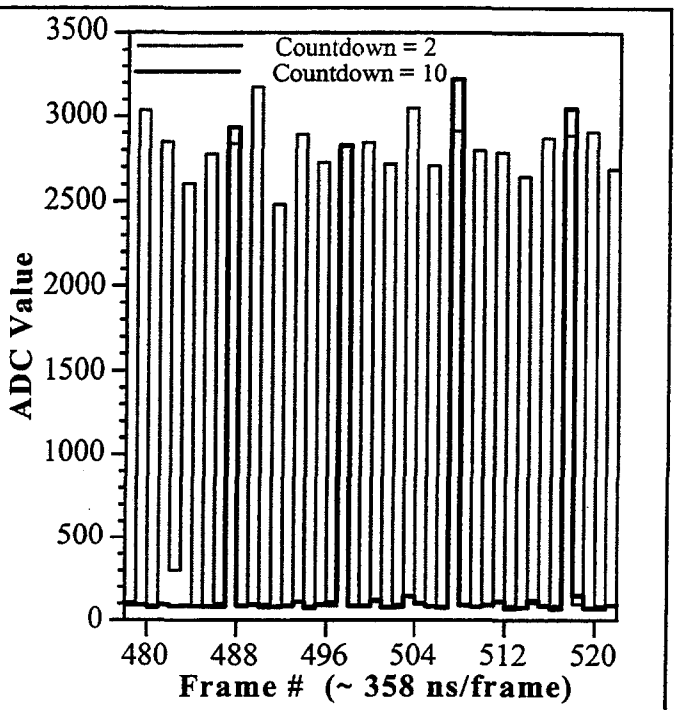

Fig. 11 Time response of the detector system for a beam burst every 2×358 ns and for a burst every 10×358 ns. The inter-frame time was 358 ns.

square subsequently superimposed on the image is the location of the detector proper as determined from the pin locations of the connectors of the detector card. The pins can be seen along all 4 edges of the image plate picture. The right hand image is a plot of the ADC values from the 64 pixels of the silicon detector and very clearly shows the resolution pattern.

Finally, Figs. 13 and 14 show the results of a dynamic experiment. The image plate inset in Fig. 13 shows a picture of a short cylindrical piece of HE seen from its side. A steel plate (the dark area) was glued to the top of the HE. At the bottom of the HE, the detonator is visible. The location of the silicon detector can be ascertained from the pins of the chip carrier. The silicon detector systems overlapped the HE with 6 or 7 rows of pixels, and overlapped the steel with two or one rows of pixels respectively. For this test both of our 8 × 8 detector systems were used, with about a 1 cm gap between them. Fig. 14 shows the output of the two systems (S1-S8 = system 1, S10-S18 = system 2). The two systems were misaligned by about one row as is evident when comparing the low numbered row regions (1-3).

Both systems had $(1\ mm)^2$ pixel detectors. For system 1, all 64 pixels were operating, whereas system 2, had four bad pixels. Fig. 13 shows the response of both of the two systems averaged over all good pixels and plotted on an arbitrarily normalized scale. The beam toroid signal is shown as the gray step function shaped curve. Also shown is the response of detector system 1 but with the individual frames normalized by the beam toroid values. The beam toroid signal shows that the beam was turned on at frame 37. A proton burst arrived once every 358 ns, the same as the frame spacing for the pixel systems. The HE was initiated at the time indicated by the vertical line at frame 146. Several μs after initiation, the detonation wave reached the region of the steel plate and began pushing it out of the field of view of the detector system. This is indicated by the steep rise in the transmitted proton beam intensity seen by the detectors. At the about same time the detonation wave broke out of the HE surfaces and the reaction products (gases) began to dissipate boosting the detector signal even more. The proton beam attenuation change due to the gas expansion is rapid at first but slows with time as the gas becomes more dilute. Nonetheless, even many hundreds of frames after the detonation, the expansion of the gas is still evident. The sudden dip starting at frame 447 is due to a 3 frame programmed interruption of the beam used to demonstrate proper operation of the system.

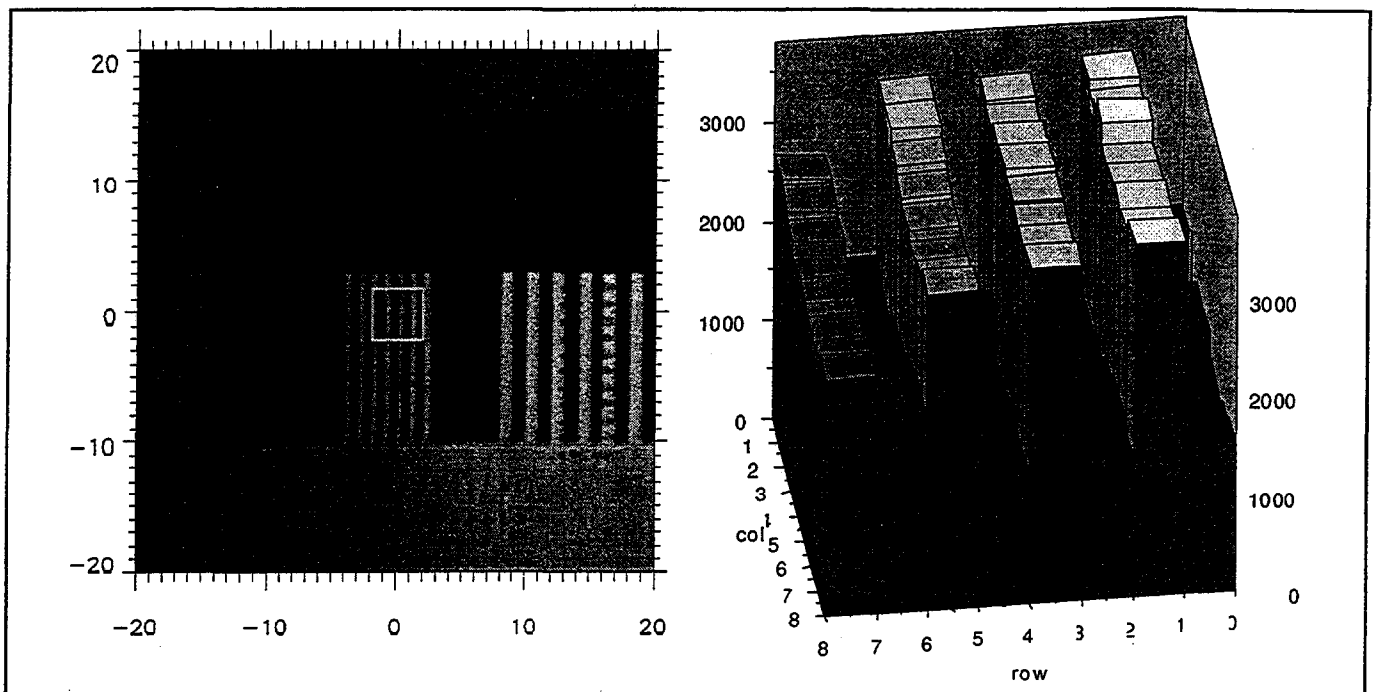

Fig. 12. The left image shows an image plate picture of a vertical resolution pattern. The scale is in mm. The two parallel rows of slightly darker small spots near all 4 edges of the image are the connector pins of the card holding the silicon detector. These were used to determine the detector location which is indicated by the small square near the center of the image. The right image shows the output of the 8 × 8 pixels in units of ADC counts.

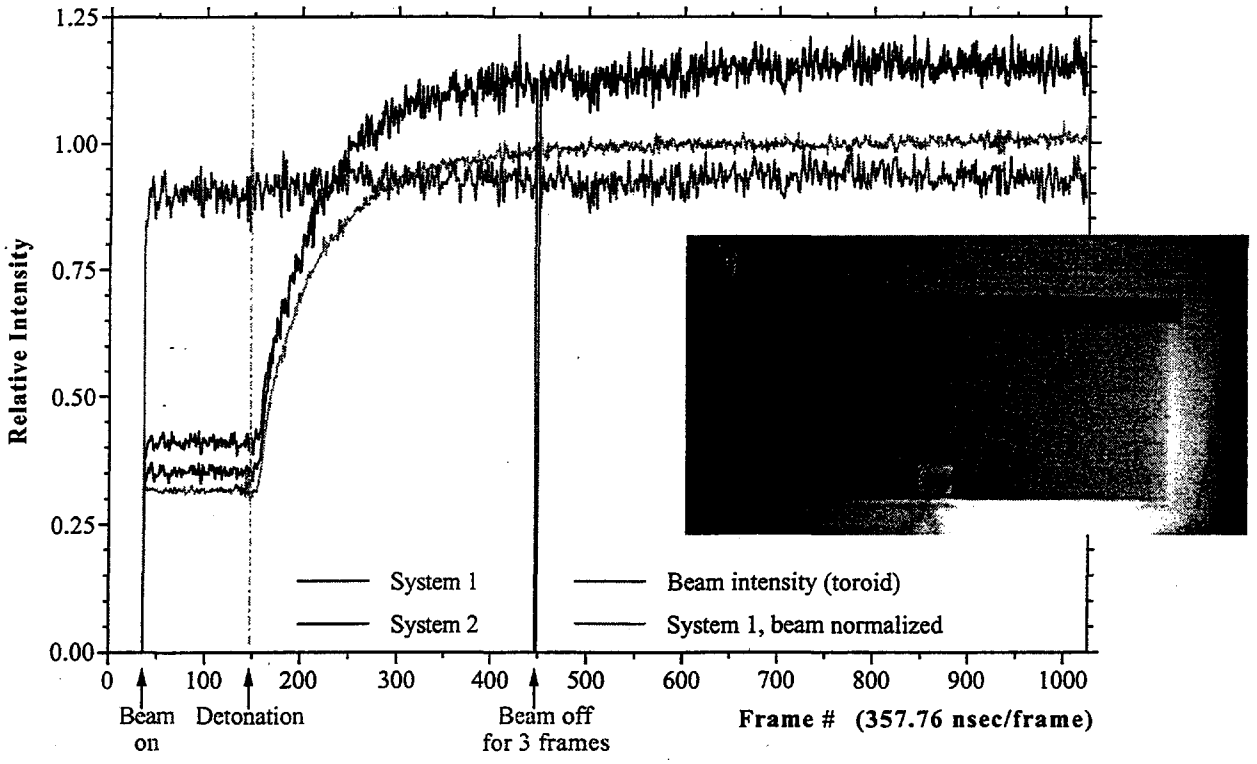

Fig. 13. The average pixel response of the detector system to the detonation of the piece of HE shown in the inset.

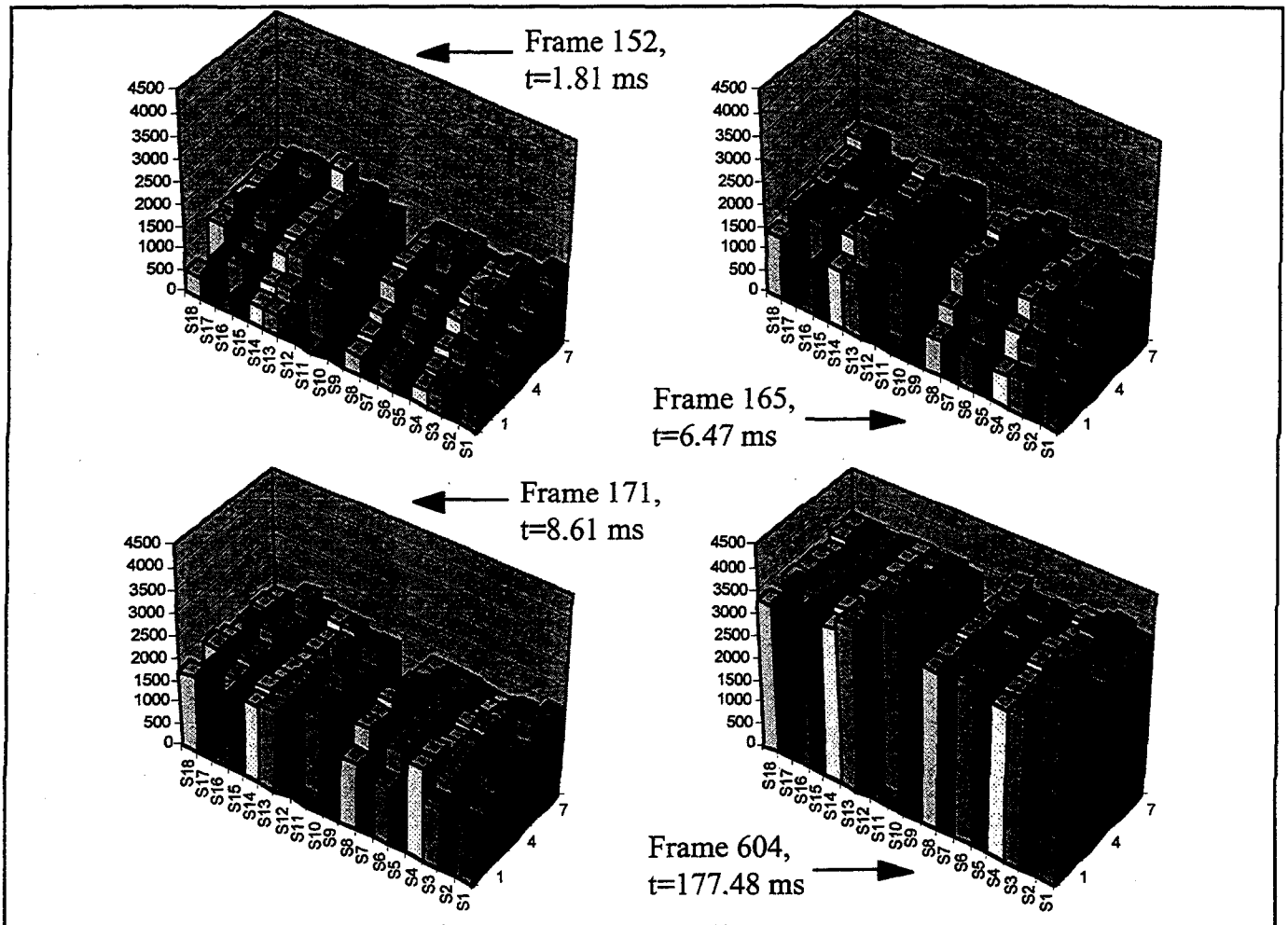

Fig. 14 Individual frames from the dynamic radiograph set shown in Fig. 13. The two 8 × 8 systems are plotted side by side.

PROBLEMS

Fig. 15 shows several sequential frames of pixel detector output of what should be a very uniform beam spot. Although this is what is seen on the average, also apparent are a number of relatively large and random fluctuations in pixel response. A systematic characterization of these fluctuations is shown in Fig. 16 in which is plotted a distribution of ratios of pixel values from a large number of frames and a large number of pixel pairs. (Frame to frame beam intensity changes, and different pixel gains were corrected for before the ratios were taken.) The rms width of the distribution is seen to be over 9%. Although there are relatively large fluctuations in energy deposition in thin detectors as given by the Landau distribution[12] or variants thereof[13] for single protons, when averaging over a large number, N, of protons per pixel, the pixel fluctuations should be a factor of $N^{1/2}$ smaller than the individual proton fluctuations. As such even a 100% fluctuation level for single proton measurements should result in only a 0.58% fluctuation in pixel response and therefore cannot be the cause of the problem. Another explanation is in order as we had $N \approx 30{,}000$ for the results shown in Fig. 15 & 16.

An alternative explanation lies in nuclear interactions of protons in the silicon pixels themselves. Starting with the inverse of the nuclear collision length in silicon of $(70.6\ g/cm^2)^{-1}$, multiplying by the density of silicon and an active detector thickness of 2.0 μm, and assuming 30,000 protons incident on a pixel in a single frame, gives a probability of 0.20 that a nuclear interaction will occur per pixel per frame. When this is folded with Poisson counting statistics, the probability of no nuclear interactions in a given pixel in a given frame is 82%, whereas 18% of the time one or more nuclear interactions take place. This is significant. One additional criterion must be satisfied for this to explain the observed effect, namely the

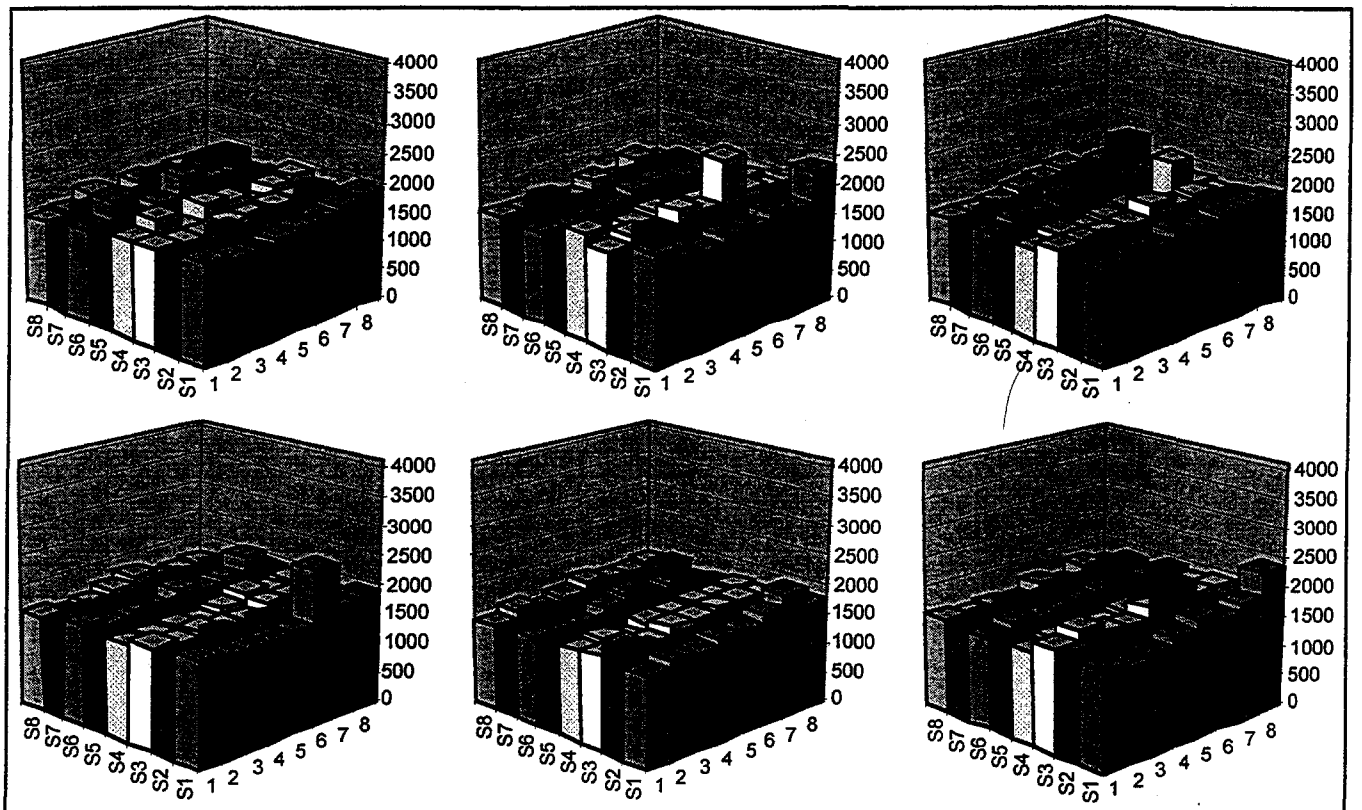

Fig. 15. Sequential frames of the smooth proton beam spot demonstrating random fluctuations in pixel response.

nuclear collision must result in a very large energy deposition in the active part of the detector. If instead the nuclear collision solely produced a single high energy secondary particle, that particle would look like any of the 30,000 incident protons and as such would result in a 1 in 30,000 part fluctuation in the signal, clearly not what is required. What is needed instead is a slow heavy recoiling particle which is capable of depositing a significant amount of its energy even in a very thin active layer. This could easily be done by a recoiling residual nuclear fragment. If we assume a knockout of a single nucleon from a silicon nucleus in which the Fermi level had a typical value (300 MeV/c), the recoiling nucleus would have an average momentum of 300 MeV/c. Translating that momentum into the kinetic energy of a mass 27 amu fragment, we find a value of 1.8 MeV, which would be easily be stopped by 2.0 μm of silicon. Comparing this energy deposit with that of the 30,000 protons, which on average each deposit about 500 eV, or 15 MeV in total, we find that a single nuclear interaction can easily cause a 12 % fluctuation. This number is of the order of magnitude required to explain the phenomenon.

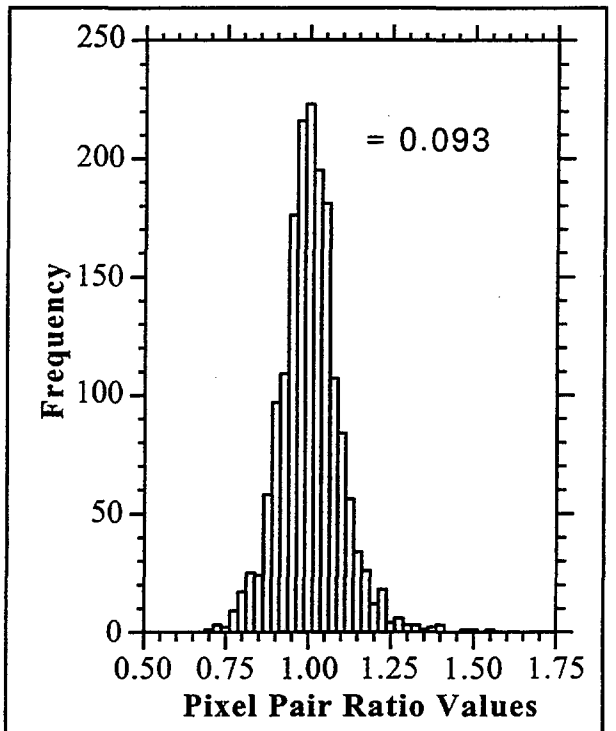

Fig. 16. Ratios of pairs of pixel values from a large number of frames and pixel pairs. Mean differences in pixel response and beam intensity were corrected for.

Several options are available to deal with this problem. A number of these are based on trying to reduce the detector thickness thereby decreasing the probability of a nuclear interaction. The limiting detector thickness value is probably around 1 μm, which would decrease the effect

by a factor of two from that calculated above. Another approach is to subdivide each resolution element in the image to a large number of pixels. One then keeps the proton beam intensity per resolution element about the same. This decreases the number of protons per pixel by the number of pixels per resolution element. The probability of a nuclear interaction per pixel changes by the same amount. While this is occurring the fractional change in signal caused by a nuclear interaction in a pixel goes up by the number of pixels/resolution element, making those "bad" pixels even more readily apparent. Those pixels are then rejected, and only the "good" pixels in a resolution element are used. If desired, the loss in the counting statistics due to the few bad pixels in a resolution element can always be compensated for by increasing the beam intensity slightly. A variant of this scheme[14] subdivides things in time as opposed to space, for instance sending 10 bursts of protons separated by 20 ns, each of 1/10th the nominal intensity and each one being read out, as opposed to 1 nominal burst every 200 ns.

An alternative to the above approach of trying to decrease the probability of a nuclear interaction is to go in the opposite direction and thereby effectively averaging out the effect of the fluctuations. For instance, in plastic scintillator, the inverse of a nuclear collision length is $1/(58.4\ gm/cm^2)$. Multiplying this by the density of the material, a thickness of 2 cm, and assuming 30,000 protons incident per pixel, one finds on the average 1000 protons have nuclear interactions. Thus the statistical effect of the interactions are reduced by a factor of $1000^{1/2}$ or about 32 over that of a single interaction. At the same time, the relative effect of a single nuclear interaction collision is greatly reduced. The normal energy deposition of a high energy proton in 2 cm of plastic scintillator is 4 MeV, about equal to the kinetic energy of a recoiling 11 amu fragment with a momentum of 300 MeV/c. The fact that this approach works can be seen by doing a pixel ratio analysis for some of the scintillator based images taken with CCD cameras discussed earlier. Such an analysis shows an rms width of just over 2%, and the majority (~80%) of that is due to the poor photon counting statistic per proton and lower number of protons per pixel.

FUTURE PLANS

Planned upgrades for the short-term CCD based system include expanding it to an 8 frame capability, and using larger diameter PFD's (40 mm vs. 25 mm) in order to increase the magnification and thereby the amount of light available and hence improving the counting statistics of photoelectrons per proton. The larger diameter PFD's will also be operated at higher voltages and therefore increased gain to make up for the loss of light that will occur in the tapered fiber optic bundle which connects the PFD to the ~ $(25\ mm)^2$ CCD. For the long-term system several paths are being pursued. We have designed an application specific integrated circuit (ASIC) which is based on the CMOS process and has been implemented in a

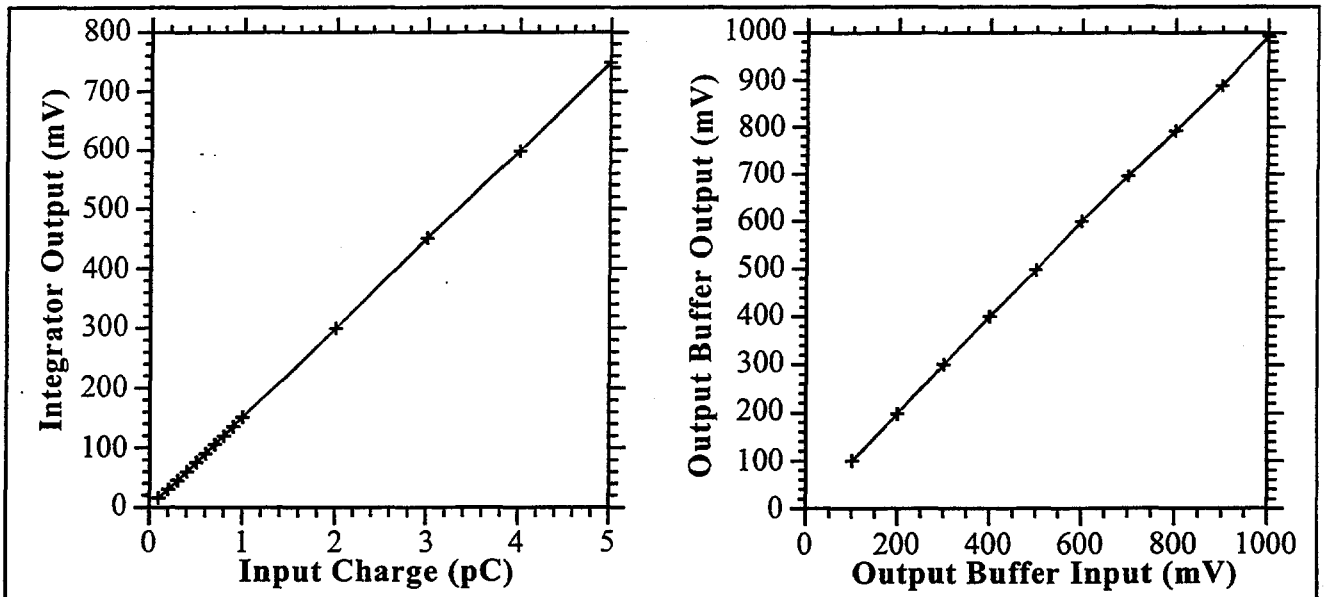

Fig. 17. Measured linearity of the response of the new ASIC chip components. The left plot is for the gated integrator and the right plot is for the output buffer circuit.

0.5 μm HP MOSIS run. The chip has 4 gated integrators which multiplex their output to an included analog memory unit. The chip then sequentially feeds the 4 analog values via a driver circuit into a separate 12 bit 40 MHz pipelined ADC. Initial performance evaluations of the ASIC chip as shown in Fig. 17 look promising. The new ADC / ASIC chip combination are planned to form the basis of a new 10,000 pixel prototype system which will be used to look at system issues. In the longer term we still need to solve the interconnect problem for $(1/4\ mm)^2$ or smaller pixels.

We will evaluate several solutions to the apparent nuclear interaction problem. We have built some small photodiode arrays compatible with the LBNL electronics, which are presently being coupled to a fiber optic array. It should be pointed out that the electronics built by LBNL were designed to be fully compatible with the use of a photodiode detector as opposed to the solid state ionization detectors. Since silicon photodiode arrays can be built much larger and more cheaply that CCD detectors, it is possible to use a lens system with unit magnification as opposed to the magnification of 1/5 that was required for the CCDs. Referring back to eq. (5), this results in about a factor 9 more light. At the same time blue sensitive photodiodes have quantum efficiencies of at least 80%[15] buying us about a factor of 4 over the photo-cathodes on our MCPs or PFDs. Using the value of 1 photoelectron per proton derived earlier for our scintillator based system, we would now be about a factor of 36 better, or at just under 1/2 the signal that would be gotten from a 1 μm thick silicon ionization detector.

Along the line of reducing the probability of nuclear collisions in a pixel in the time domain, we are considering building a version of the electronics which would use a single 40 MHz ADC to look at individual pixels once every 30 to 40 ns. We will also look at reducing the detector thickness to 1 μm.

CONCLUSIONS

We have constructed a 4 frame electro-optically gated CCD based camera system capable of operating at speeds of better than 1 frame/μs, and producing high resolution images. This system is already being used to evaluate the proton radiography concept. We have also designed, built, and beam tested a 64 pixel silicon detector based system that meets all the current performance requirements for the final AHF system with the exception of pixel size and some aspects of noise performance. The noise performance issue is apparently not in the electronics, but instead is linked to nuclear interactions of the probing proton beam in the detector and the very high proton beam intensity we have. Several solutions to this problem seem to exist and will be evaluated in detail in the near future.

---

[1] H.-J. Ziock et al., "The Proton Radiography Concept", these proceedings.

[2] H. Bichsel, Nucl. Instr. and Meth. **B52** (1990) 136.

[3] C. T. Mottershead and J. D. Zumbro, "Magnetic Optics For Proton Radiography", Proceedings of the Particle Accelerator Conference, Vancouver, Canada, May 1997.

[4] IMCO ELECTRO-OPTICS, LTD., 14/16 Safron Ct., Southfiled Industrial Park, Basildon, Essex SS15 6SS, UK.

[5] "Measured Responsivities of Generation II and Hybrid Image Intensifiers", G. J. Yates and Nicholas S. P. King, SPIE Vol. 2551, Photoelectronic Detectors, Cameras, and Systems, pp. 145–158, July 13–14, 1995, San Diego, California.

[6] N. S. P. King, G. J. Yates, S. A. Jaramillo, J. W. Ogle, and J. L. Detch Jr., "Nanosecond Gating Properties of Proximity-Focused Microchannel-Plate Image Intensifiers", Los Alamos Conference on Optics, SPIE Vol. 288, pp. 426–433, April 7-10, 1981, Santa Fe, New Mexico.

[7] See for instance H. W. Funk, "Introduction to Image Intensifier Tubes", PROXITRONIC, Robert-Bosch Str. 34, D-64625 Bensheim, Germany.

[8] Directed Energy Inc., 2401 Research Blvd, Suite 108, Fort Collins, CO 80526, USA.

[9] Delft Electronic Products BV,P.O.Box 60 , NL 9300AB Roden, The Netherlands.

[10] G. J. Yates et al., "An Intensified/Shuttered Cooled CCD Camera for Dynamic Proton Radiography", Proceedings of Electronic Imaging '98 Conference, 24-30 January 1998, San Jose, CA.

[11] Lawrence Semiconductor Research Laboratory, Inc., 2300 West Huntington Drive, Tempe, Arizona 85282, USA.

[12] L. Landau, J. Phys. USSR **8** (1994) 201.

[13] H. Bichsel and R. P. Saxon, Phys. Rev., **A11** (1975) 1286.

[14] E. Moore, U. of New Mexico, USA, private communication.

[15] Hamamatsu Corporation S4753-02 photodiode, typical QE @425 nm is 82% (0.28 A/W).